JOURNAL OF SOLID STATE CHEMISTRY 20, 143–148 (1977)

Structural Aspects and Defect Chemistry in In_2O_3

J. H. W. DE WIT

Inorganic Chemistry Department, University of Utrecht, Croesestraat 77A, Utrecht, The Netherlands

Received July 12, 1976; in revised form September 10, 1976

The *C*-type rare earth structure of In_2O_3 is compared with the fluorite structure. The stability of the structure is discussed based on DTA and X-ray work and electron microscopy. Ordering of defects does not take place, so that defect chemistry can be formulated for isolated defects in nonstoichiometric In_2O_3. The influence of the incorporation of aliovalent cations into the In_2O_3 host lattice is discussed and a defect model is suggested.

Introduction

Under normal conditions, In_2O_3 crystallizes in the *C*-type rare earth structure (T_h^7, *Ia*3). This structure has been known since 1930 (*25*). Since then it has been refined by means of X-ray measurements (*3*, *4*, *7*, *9*) and neutron diffraction (*26*). This formation of solid solutions with various materials, and the influence of the incorporation of aliovalent cations on several parameters like the electrical conductivity and the infrared reflectivity, have been described by various authors (*14*, *15*, *20–24*). The defect chemistry of In_2O_3 has hardly been discussed and the incorporation mechanism of the impurities is unknown. It is the purpose of this paper to improve this situation.

Stability of the Structure

In_2O_3 crystallizes in the *C*-type rare earth structure. This means that the structure is body centered cubic with 80 atoms per unit cell. X-ray measurements gave a unit cell dimension of 10.100 ± 0.005 Å, in good agreement with literature data (*1–3*). This structure is closely related with the fluorite structure. In In_2O_3 every fourth anion is missing, so that small shifts of the ions take place (~4%). At first sight the close relation with the fluorite structure suggests a rather easy transformation from the *C*-type atom position to the fluorite positions. One can expect the formation of solid solutions with other oxides having the fluorite structure, like ZrO_2, CeO_2, and HfO_2. However, no evidence was found in the literature that the atoms in In_2O_3 would take fluorite positions. At 65 kbar and 1000°C the *C*-type structure of In_2O_3 is transformed to the corundum structure (*5*, *6*), while at 111 kbar and 1100°C it crystallizes in a perovskite-like structure, with the In^{+3} ions on both the *A* and *B* sites (*9*). Both structures are metastable with respect to the *C*-type rare earth structure at atmospheric conditions. Annealing at 1200°C respectively, 800°C showed both phases to transform to the *C*-type structure (*6*, *9*). A transformation to the *A*-type or *B*-type rare earth structure, which is not uncommon for the *C*-type structure, may take place only at very high temperatures, as would be expected for the small cation radius of In^{3+} (*10*).

DTA experiments that we performed on In_2O_3 up to 1500°C did not show any phase change, which is in accordance with the expected behavior. (The melting point of In_2O_3 is at about 1900°C.) Reduction of the material with hydrogen did not deliver any other phases than *C*-type In_2O_3 and metallic In, which was verified with X-ray analysis.

ISSN 0022-4596

TG measurements in an oxygen atmosphere up to 1400°C did show only a very small loss of oxygen (*8*), resulting in In_2O_{3-x} with x of the order of 0.01 at 1400°C. This indicates the relative stability of the stoichiometric material.

We also checked the possibility of the ordering of oxygen vacancies. Some authors (*11*, *12*) suggested the existence of oxygen vacancies (with respect to the 2/3 cation/anion ratio), because of the irregularity of the MO_6 coordination groups. Aleshin and Rustum Roy (*12*) discussed the possibility of a disorder–order transition in going from the fluorite (M_4O_8) via the pyrochlore (M_4O_7) to the *C*-type rare earth structure (M_4O_6). However, they did not arrive at a definite conclusion. The empty oxygen site arrangement in In_2O_3 with respect to the fluorite structure cannot be rationalized in terms of any one simple low index set of planes (*13*). No indication for any kind of vacancy ordering or any other defect ordering, either for stoichiometric In_2O_3 or for partly reduced In_2O_3 could be observed by means of electron microscopy and diffraction.[1] We therefore conclude that the In_2O_3 *C*-type rare earth structure is a very stable one.

The incorporation of In^{3+} ions ($r = 0.78$ Å) in interstitial positions is very well possible, in principle, as was calculated from a hard sphere model. This is sustained by the oxidation rate measurements of Rosenberg (*16*, *17*) at 308–407°C on In metal, which showed the the existence of In^{3+} in interstitial positions. On the other hand, oxygen vacancies might be possible as well.

As we have shown before (*8*) the possible contribution of $In_i^{\cdots}$ to the conductivity is below 0.1%. Because of the insensitivity of the electrical conductivity on the frequency (*18*) possible oxygen vacancies also will not be very mobile, as is sustained by the clear oxygen pressure dependence of the conductivity. However, at high temperature (>800°C) they might be present at a reasonably high concentration and mobile enough to obscure our quenching experiments on polycrystalline material as described elsewhere (*18*). When quenching single crystals, the high temperature situation could be frozen, which was also visible by the color of the crystals. When cooling was performed more slowly (several hours) oxygen was taken up by the lattice again, resulting in more transparent crystals again. No difference between the surface layer and the bulk of the crystals could be observed; a fact which supports the oxygen vacancy model (*19*).

From this discussion it follows that the classical defect chemistry may be applied to In_2O_3, without disturbance by ordering of defects. As to the nature of the majority ionic defects, we are now in contradistinction with our earlier expectations (*27*), and are inclined to accept the oxygen vacancy model. But we will not exclude the possibility of the presence of In^{3+} in interstitial positions. Their concentration, however, is probably smaller than the oxygen vacancy concentration. In the rest of this paper we use the oxygen vacancy model, which as we shall see is sustained by our doping experiments.

The Incorporation of Alien Cations in In_2O_3

Some literature data concerning the incorporation of alien cations into In_2O_3 are compiled in Table I. The color of In_2O_3 doped with tetravalent cations changes from pale yellow to yellow-green, with increasing concentration, a phenomenon that we also observed. On the other hand, the undoped flux grown crystals of Chase and Tippins (*22*), which showed a very dark color, changed to yellow when doped with divalent Mg^{2+}

TABLE I

THE INCORPORATION OF ALIEN CATIONS INTO THE In_2O_3 LATTICE

Cation	Composition	Color	Reference
Zr^{4+}	5 at%	Yellow	*21*
Sn^{4+}	3 wt%	Green	*21*
Ti^{4+}	5 wt%	Yellow	*21*
Mg^{2+}	0.16 wt%	Green	*22*
Mg^{2+}	0.23 wt%	Yellow	*22*

[1] These experiments were kindly performed for us by Prof. S. Amelynckx, Rijksuniversitair Centrum te Antwerpen, Belgium.

ions. This color change was also observed by us. When heating these samples to a temperature of 1400°C, after which quenching was performed, the color changed back to nearly black. This color change was reflected in the higher conductivity of the samples (*8*). The same parallel between the dark color resulting from the incorporation of tetravalent cations and the increasing conductivity is discussed by Groth (*24*), who observed a clear increase of the electron concentration as a function of the incorporated amount of tetravalent cations like Sn^{4+} and Zr^{4+}. We did observe a decrease of the electronconcentration as a function of the amount of incorporated Mg^{2+} or Ca^{2+}. We will now discuss the defect chemistry resulting from this incorporation.

Experimental

Doping Procedure

To 1 g of pure In_2O_3 powder (Cerac/Pure, 99.999%), a carefully weighed amount of MO (M for Mg or Ca) is added to reach a 3000 ppm (wt) concentration of M. This mixture is stirred thoroughly in 100 ml of deionized water for 20 hr in a polyethylene vessel. Thereafter the mixture is dried in air at 140°C for 40 hr. The powder is then ground in a ball mill for 1 hr. The powder is pressed into a tablet using a pressure of 3 tons cm^{-2}, whereafter the tablet is sintered on an Al_2O_3 plate at 1300°C in air for 8 hr. The sintered tablet is then ground again in the ball mill, and 0.1 g of the resulting powder is added to 0.9 g of the pure In_2O_3 to reach a 10-fold lower dope concentration. With this mixture the same procedure is followed as with the original 3000-ppm sample. In this way several lower concentrations were prepared. The resultant dope concentration as a function of the added amount has been plotted in Fig. 1.[2]

The Electrical Conductivity Measurements

The measurements of electrical conductivity have been described before (*27*). The conductivity decreased with increasing M content. The best information on the incorporation mechanism would result from direct measurements of the electron concentration as a function of the M content, e.g., via Hall experiments. However, we could only measure the Hall effect up to 700°C in an oxygen-containing atmosphere where chemisorption of oxygen influences the electron concentration to a great extent, as we will show in another paper (*18*). Therefore, we used electrical conductivity experiments in vacuum (10^{-9} to 10^{-5} atm), to exclude the effect of chemisorption. Thereby the samples were always heated to 1000°C before cooling to the measuring temperature. This of course leaves us with a possible influence of the carrier concentration dependence of the mobility, when measuring the conductivity at one temperature as a function of the M content. However, for our doped samples the electron concentration was below 10^{18} cm^{-3}. This makes the mobility rather insensitive to changes in the carrier concentration, so that the slope of the log σ vs log M plot can be interpreted as if it were a log n vs log M plot.

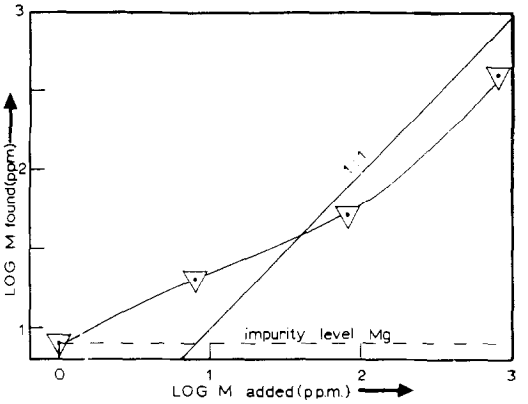

FIG. 1. The logarithms of the experimentally found M concentrations as functions of the amounts added.

Defect Chemistry

The nonstoichiometric decomposition of In_2O_3 can be described by (*18*):

$$2\,In_{In}^{x} + 3\,O_O^{x} \rightleftarrows 2\,In_{In}^{x} + 3\,V_{\dot{O}}^{\cdot} + 6e' + \tfrac{3}{2}O_2 \qquad (1)$$

with an equilibrium constant

$$K_{ox} = [V_{\dot{O}}^{\cdot}]^3 \cdot n^6 \cdot P_{O_2}^{+\frac{3}{2}}, \qquad (2)$$

where n denotes the electron concentration.

[2] The analyses were carried out in the Philips Research Laboratories in Eindhoven, The Netherlands.

Because we observed a decrease in the conductivity of In_2O_3 when doped with Mg^{2+} of Ca^{2+} (from here we shall usually write M^{2+} because we did not observe a different behavior for these two cations), the M^{2+} cation is not incorporated in an interstitial position but must have been incorporated substitutionally on In sites. Therefore, we propose the following incorporation mechanism:

$$2MO \rightarrow 2M'_{In} + 2O_O^x + V_O^{\cdot\cdot}, \quad (3)$$

and at high partial oxygen pressure;

$$2MO + \tfrac{1}{2}O_2 \rightarrow 2M'_{In} + 3O_O^x + 2p, \quad (4)$$

where p denotes the hole concentration.

The electroneutrality equation can be represented by

$$n + [M'_{In}] + 3[V''_{In}] = p + 2[V_O^{\cdot\cdot}], \quad (5)$$

or

$$n + [M'_{In}] + 2[O''_i] = p + 2[V_O^{\cdot\cdot}], \quad (5')$$

depending on the existence of a Schottky defect situation for Eq. (5) or a Frenkel disorder on the anion sublattice for Eq. (5'). For our purpose the choice between the two models is irrelevant, because we assume that the oxygen vacancy concentration is relatively large so that: $[V_O^{\cdot\cdot}] \gg [O''_i]$ or $[V'''_{In}]$. We will therefore neglect $[V'''_{In}]$ and $[O''_i]$ in Eqs. (5) and (5'), which may only influence our results at high oxygen pressures. The electroneutrality condition becomes

$$n + [M'_{In}] = p + 2[V_O^{\cdot\cdot}]. \quad (6)$$

At low oxygen pressures (range 1 in Fig. 2), this equation simplifies to

$$n = 2[V_O^{\cdot\cdot}],$$

which combined with Eq. (2) delivers

$$n \sim P_{O_2}{}^{-0.166} \quad \text{and} \quad [V_O^{\cdot\cdot}] \sim p_{O_2}{}^{-0.166},$$

and because $n \cdot p = k_i$, where k_i denotes the intrinsic electron hole product:

$$p \sim p_{O_2}{}^{+0.166}.$$

At higher oxygen pressures (range 2) Eq. (6) becomes

$$[M'_{In}] = 2[V_O^{\cdot\cdot}].$$

Combining this with Eq. (2) gives

$$n = 1.41\, K_{ox}{}^{\frac{1}{6}} \cdot p_{O_2}{}^{-\frac{1}{4}} \cdot [M'_{In}]^{-\frac{1}{2}} \quad (7)$$

and

$$p \sim p_{O_2}{}^{+\frac{1}{4}} \cdot [M'_{In}]^{+\frac{1}{2}}.$$

The transition from range 1 to 2, where $n = 2[V_O^{\cdot\cdot}] = [M'_{In}]$, takes place at

$$p_{O_2}{}^{1\rightarrow 2} = \frac{\{8K_{ox}\}^{\frac{1}{3}}}{[M'_{In}]^6}. \quad (8)$$

At still higher oxygen pressures (range 3) Eq. (6) becomes

$$p = [M'_{In}].$$

This implies that n and p are no function of the partial oxygen pressure. Combining this with Eq. (2) gives

$$[V_O^{\cdot\cdot}] = \frac{K_{ox}{}^{\frac{1}{3}} \cdot [M'_{In}]^2}{k_i{}^2 \cdot p_{O_2}{}^{\frac{1}{2}}}. \quad (9)$$

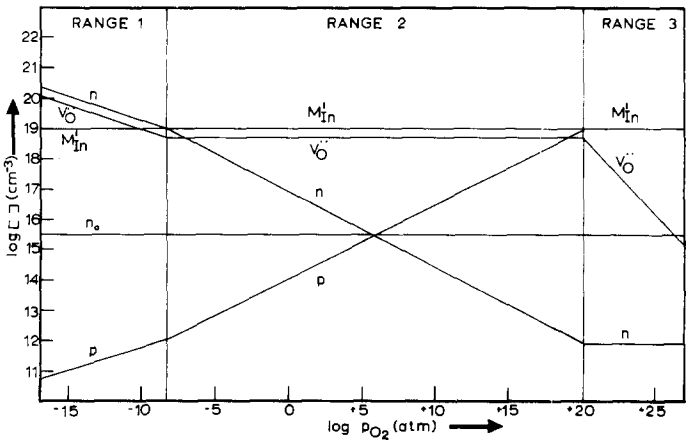

FIG. 2. A Kröger–Vink diagram for In_2O_3 at 800°C with a dopant concentration of 10^{19} M'_{In} cm^{-3}.

The transition from range 2 to 3, where 2 $[V_O^{\cdot\cdot}] = [M'_{In}] = p$, takes place at

$$p_{O_2}^{2\to3} = \frac{\{8K_{ox}\}^{\frac{1}{2}} \cdot [M'_{In}]^2}{k_i^4}. \qquad (10)$$

At extremely high pressures, a fourth range may exist, where $p = 3[V'''_{In}]$ or $p = 2[O''_i]$, which we will not discuss. The transition from range 1 to 2 and from range 2 to 3 is not a sharp one. For the transition region of range 1 to 2, Eq. (6) should read: $[M'_{In}] + n = 2[V_O^{\cdot\cdot}]$, which gives

$$\left\{\frac{n_0}{n}\right\}^2 - \frac{n}{n_0} = \frac{[M'_{In}]}{2[V_O^{\cdot\cdot}]_0} \qquad (11)$$

for the dope concentration dependence of n. The subscript o refers to the concentrations in undoped samples.

Figure 2 shows a Kröger–Vink diagram, where the logarithms of the carrier concentrations have been plotted as a function of the logarithms of the partial oxygen pressures. This figure is valid for a temperature of 800°C and for $[M'_{In}] = 10^{19}$ cm^{-3}. This plot has been calculated using the above equations with

$$K_{ox}^{(1073K)} = 10^{+157.6}\ \text{cm}^{-26}\ \text{atm}^{+\frac{1}{2}},$$

and

$$k_i^{(1073K)} = 1.1 \times 10^{+31}\ \text{cm}^{-6}.$$

These values have been published before (*8*, *18*). As can be seen in this figure the normal experimental pressure region lies in range 2. This predicts a $[M'_{In}]^{-\frac{1}{2}}$ dependence of the electron concentration (cf. Eq. (7)).

Figure 3 shows the $[M'_{In}]$ concentration dependence of the electron concentration for various pressures at 800°C. It is obvious that at low pressures a $[M'_{In}]^{-\frac{1}{2}}$ dependence can only be expected for the higher dope concentrations. For a temperature of 800°C, we only observed a clear decrease of the conductivity when doped with 8×10^{19} $[M'_{In}]$ cm^{-3}, our highest dope concentration. Therefore, we should like information on the dope dependence at a lower temperature, where $[V_O^{\cdot\cdot}]_0$ is smaller. Because cooling under vacuum does not deliver an equilibrium situation, we were not able to measure dope dependence at lower temperatures, e.g., 500–600°C, under vacuum with a defined $[V_O^{\cdot\cdot}]_0$. Although we may not be able to indicate with whiche quilibrium temperature the $[V_O^{\cdot\cdot}]_0$ corresponds, we are certain that no interaction with the bulk of the material takes place below 500°C (*18*). Thus we conclude that the $[V_O^{\cdot\cdot}]_0$, after cooling to room temperature under vacuum, corresponds with a temperature between 500 and 800°C.

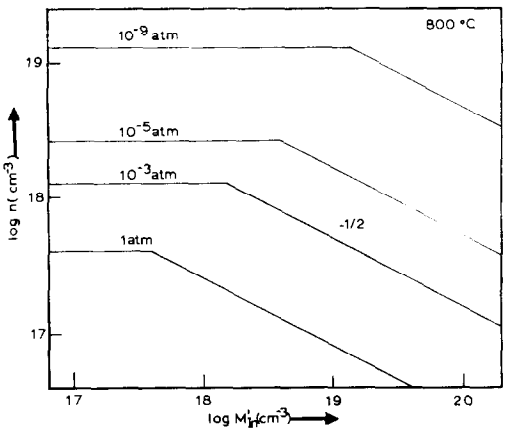

FIG. 3. The electron concentration as a function of the M'_{In} concentration for various partial oxygen pressures at 800°C.

When we plot log σ vs log $[M'_{In}]$ we now observe a clear concentration dependence from 4×10^{18} cm^{-3} onwards. The slope of the curve (see Fig. 4) is in good agreement with our proposed incorporation model.

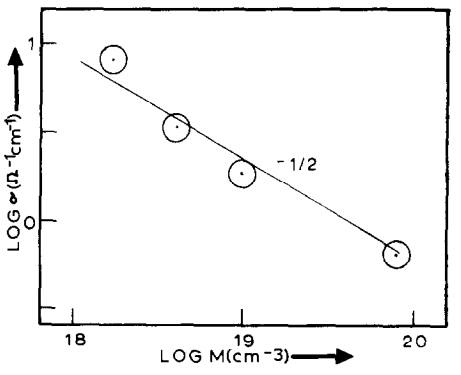

FIG. 4. The logarithms of the experimentally found electrical conductivities as functions of the logarithms of the experimentally verified Mg concentrations.

For the samples doped with 8×10^{19} $[M'_{In}]$ cm^{-3}, we also measured the dependence of $\log \sigma$ on $\log p_{O_2}$, which should theoretically give an exponent of -0.25 for our samples at 800°C, between 10^{-3} and 10^{0} atm. Experimentally we observed an exponent of $-(0.23 \pm 0.02)$. At higher temperatures this exponent decreased to (0.19 ± 0.02) at 870°C. From Fig. 2 we can read that the electron concentration at 800°C in the pressure range from 10^{-3} to 1 atm, does not reach 10^{18} cm^{-3}. However, for higher temperatures this concentration increases, so that the starting degeneracy of the carrier concentration may disturb the results, because the law of mass action may no longer be applied. This results in an effectively lower exponent.

For the alternative defect model based on $In_i^{\cdots}$ as the majority ionic defect, a similar picture can be built up. But there the expected exponent in the $\log \sigma$ vs $\log [M'_{In}]$ plot would be $-\frac{1}{3}$, which is not in accordance with our measurements.

Conclusions

The *C*-type rare earth structure of In_2O_3 was shown to be very stable. Defect ordering in this structure is not expected, as was checked with electron microscopy. Therefore, the incorporation of aliovalent cations can be described with classical defect chemistry. The incorporation of tetravalent cations enhances the electron concentration, while divalent cations diminish it.

The $\log \sigma$ vs $\log [M'_{In}]$ plot shows an exponent of $-\frac{1}{2}$. This is in agreement with our incorporation model, based on the existence of oxygen vacancies as the majority of ionic defects. The oxygen pressure dependence of the conductivity sustains this model.

Acknowledgments

The present investigations have been carried out under the auspices of the Netherlands Foundation for Chemical Research (SON) and with financial aid from the Netherlands Organization for the Advancement of Pure Research (ZWO).

The author is indebted to Prof.-Dr. W. van Gool for critically reading the manuscript and to Dr. J. Schoonman of the Solid State Chemistry Department of this University for providing us with the drawings of the high-temperature conductivity cell.

References

1. R. S. Roth, *J. Res. Nat. Bur. Stand.* **58**, 75 (1957).
2. R. Roy and M. W. Shafer, *J. Phys. Chem.* **58**, 372 (1954).
3. E. Staritzky, *Anal. Chem.* **28**, 4, 553 (1956).
4. M. Marezio, *Acta Crystallogr.* **20**, 723 (1966).
5. R. D. Shannon, *Solid State Comm.* **4**, 629 (1966).
6. A. Nørlund Christensen and N. C. Broch, *Acta Chem. Scand.* **21**, 1046 (1967).
7. R. S. Roth and S. J. Schneider, *J. Res. Nat. Bur. Stand.* **64A**, 309 (1960).
8. J. H. W. de Wit, *J. Solid State Chem.* **13**, 192 (1975).
9. M. Marezio, A. Waintal, J. Chenavas, J. J. Capponi, and M. Gondrand, *Colloq. Int. Centr. Nat. Rech. Sci.* **188**, 403 (1970).
10. R. D. Shannon and C. T. Prewitt, *Acta Crystallogr.* **B26**, 1046 (1970).
11. LeRoy Eyring and Bo Holmberg, *in* "Nonstoichiometric Compounds," Chap. 4, Advances in Chemistry Series, No. 39, (1963), Am. Chem. Soc.
12. E. Aleshin and R. Roy, *J. Amer. Ceram. Soc.* **45**, 1, 18 (1962).
13. A. W. Mann, *J. Solid State Chem.* **11**, 94 (1974).
14. J. C. Wallmann, *J. Inorg. Nucl. Chem.* **26**, 2053 (1964).
15. G. Gashurov and O. J. Sovers, *Acta Crystallogr.* **26**, 938 (1970).
16. A. Rosenberg, *J. Phys. Chem.* **64**, 1143 (1960).
17. A. Rosenberg and M. C. Lavine, *J. Phys. Chem.* **64**, 1135 (1960).
18. J. H. W. de Wit, G. van Unen, and M. Lahey, to be published.
19. M. F. Berard and D. R. Wilder, *J. Appl. Phys.* **34**, 2318 (1963). M. F. Berard and D. R. Wilder, *J. Amer. Ceram. Soc.* **52**, 85 (1969).
20. I. A. Rozdin et al., *Izv. Akad. Nauk. SSSR Neorg. Mater.* **7**, 10, 1798 (1971).
21. R. J. Bones and J. Woodhead, German Patent, Offenlegungsschrift 2127135 (16. Dez. 1971).
22. A. B. Chase and H. H. Tippins, *J. Appl. Phys.* **38**, 6, 2469 (1967).
23. C. Schusterius and N. N. Padurov, *Ber. Deut. Keram. Ges.* (H10) **30**, 235 (1953).
24. R. Groth, *Phys. Status Solidi* **14**, 69 (1966).
25. L. Pauling and M. D. Shappell, *Z. Kristallog.* **75**, 128, (1930).
26. M. Betzl et al., *Z. Kristallog.* **118**, 473 (1963).
27. J. H. W. de Wit, *J. Solid State Chem.* **8**, 142 (1973).